Journal of Power Sources 248 (2014) 323–329

Contents lists available at ScienceDirect

Journal of Power Sources

journal homepage: www.elsevier.com/locate/jpowsour

$Li_{4-x}Na_xTi_5O_{12}$ with low operation potential as anode for lithium ion batteries

C.W. Xiao [a,b], Y. Ding [a], J.T. Zhang [a], X.Q. Su [b], G.R. Li [a], X.P. Gao [a,*], P.W. Shen [a]

[a] Institute of New Energy Material Chemistry, Synergetic Innovation Center of Chemical Science and Engineering (Tianjin), Tianjin Key Laboratory of Metal and Molecule Based Material Chemistry, Nankai University, Tianjin 300071, China
[b] Tianjin Institute of Power Sources, Tianjin 300381, China

HIGHLIGHTS

- The substitution of lithium ions by sodium ions leads to the phase transformation.
- The $Li_2Na_2Ti_5O_{12}$ presents the low and sloped potential plateau.
- The $Li_2Na_2Ti_5O_{12}$ delivers the good high-rate capability and cycle stability.

ARTICLE INFO

Article history:
Received 8 August 2013
Received in revised form
29 September 2013
Accepted 30 September 2013
Available online 6 October 2013

Keywords:
Lithium-ion batteries
Anode
Spinel
Sodium
Substitution

ABSTRACT

In this work, the unique effect of the substitution of lithium ions by sodium ions in $Li_4Ti_5O_{12}$ on the structure, crystalline size and electrochemical performance is investigated in details. The $Li_{4-x}Na_xTi_5O_{12}$ materials are by high temperature calcination of titania, anhydrous lithium carbonate and anhydrous sodium carbonate. It is shown from the structure analysis that the phase structure transformation is found with gradually increasing the molar ratio of sodium ions to lithium ions in the as-prepared $Li_{4-x}Na_xTi_5O_{12}$ samples, accompanied with the evident growth of the crystallites. Because of the phase structure transformation from a cubic structure to an orthorhombic structure whose open relatively tunnel structure along the *b*-axis makes for the lithium ion insertion/extraction, the $Li_2Na_2Ti_5O_{12}$ sample presents the low and sloped potential plateau as expected, distinguished from the high and flat potential plateau of $Li_4Ti_5O_{12}$. Meanwhile, the $Li_2Na_2Ti_5O_{12}$ sample delivers the good high-rate capability and cycle stability during cycling. The results clarify the positive effect of the suitable substitution of lithium ions by sodium ions in $Li_4Ti_5O_{12}$ anode material with the low operation potential for insuring the high working voltage of lithium ion batteries.

1. Introduction

The safety issue is important for high-power and high-energy lithium ion batteries in electric vehicles (EVs) [1–3]. Among those safe alternatives to graphite anode, $Li_4Ti_5O_{12}$ is of particular interest due to its high operation potential plateau at about 1.5 V vs Li/Li^+ to avoid the lithium dendrite growth, and negligible volume change in the lithium insertion/extraction processes to ensure long cycle stability [4–6]. Therefore, extensive investigation has been made to fabricate nanostructured $Li_4Ti_5O_{12}$ or $Li_4Ti_5O_{12}$/carbon composites based on the requirement for high power lithium ion batteries [7–20].

Usually, lithium ion batteries with a high safety are coupled with $Li_4Ti_5O_{12}$ anode and $LiFePO_4/LiMn_2O_4/LiCoO_2$ cathode [21–23]. However, such batteries suffer from the low working voltage due to the high operation potential of $Li_4Ti_5O_{12}$ anode, resulting in the low energy density of batteries. In order to increase the working voltage and energy density of lithium ion batteries, one way is to use cathode materials with higher operation potential in batteries, such as $LiNi_{0.5}Mn_{1.5}O_4$, $LiMnPO_4$ and $LiCoMnO_4$ [24–26]. Another way is to depress the operation potential of Ti-based compounds as anode to insure the high working voltage of lithium ion batteries. Meanwhile, it should be noted that lithium ions in $Li_4Ti_5O_{12}$ anode are electrochemically inactive in the two-phase reaction between $Li_4Ti_5O_{12}$ with a cubic spinel

* Corresponding author. Tel./fax: +86 22 23500876.
E-mail address: xpgao@nankai.edu.cn (X.P. Gao).

0378-7753/$ – see front matter © 2013 Elsevier B.V. All rights reserved.
http://dx.doi.org/10.1016/j.jpowsour.2013.09.131

structure and $Li_7Ti_5O_{12}$ with an ordered rock-salt structure [5]. Based on the effective utilization of lithium resources in lithium ion batteries [27], it is significant to replace inactive lithium ions with abundant cations in Ti-based compounds [28–34], such as sodium and magnesium ions. In particular, the sodium ions are much more abundant as compared with lithium resources in the earth's crust. In addition, the radius of sodium ions is obviously larger than that of lithium ions. When lithium ions are partially substituted by sodium ions in Ti-based compounds, it would be beneficial to fabricate new anode host materials with a relatively open tunnel structure for decreasing the operation potential in the lithium insertion/extraction processes.

In this work, lithium ions are substituted gradually by sodium ions in $Li_4Ti_5O_{12}$, prepared by the high temperature calcination of titania, anhydrous lithium carbonate and anhydrous sodium carbonates. The microstructure, size, and electrochemical performances of the as-prepared Ti-based anode materials are analyzed and discussed to reveal the effect of ion substitution on the structure and operation potential.

2. Experimental

2.1. Preparation and characterization

The $Li_{4-x}Na_xTi_5O_{12}$ ($0 \le x \le 4$) samples, in which the stoichiometric formula only expressed molar amount of the used elements in the starting materials, were prepared by the simple high temperature solid-phase reaction. Anhydrous lithium carbonate, anhydrous sodium carbonate and the commercial titania (P25, Degussa) were mixed with various molar ratio and adequately grinded in an agate mortar. The resulting mixtures were calcined at 750 °C for 2 h in air to obtain the final $Li_{4-x}Na_xTi_5O_{12}$ samples. According to the different molar ration of the elements, the as-prepared five samples in this work were designated as $Li_4Ti_5O_{12}$, $Li_3NaTi_5O_{12}$, $Li_2Na_2Ti_5O_{12}$, $LiNa_3Ti_5O_{12}$ and $Na_4Ti_5O_{12}$, respectively.

Phase identification of the $Li_{4-x}Na_xTi_5O_{12}$ samples was determined by X-ray diffraction (XRD, Rigaku MiniFlex II) with a range of 2θ from 10 to 80° at a rate of 5° min^{-1}. The morphology and microstructure of the samples was characterized by scanning electron microscopy (SEM, Hitachi S-4800) and transmission electron microscopy (TEM, FEI Tecnai F20).

2.2. Electrochemical measurements

The obtained samples, acetylene black, and binder (polytetrafluoroethylene, PTFE) were mixed at a weight ratio of 75:15:10, and compressed to prepare the working electrode. Metallic lithium was used as the counter and reference electrodes. $LiPF_6$ (1 M) in the mixture solution composed of ethylene carbonate (EC) and dimethyl carbonate (DMC) with a volume ratio of 3:7 was used as electrolyte. The galvanostatic method was used to measure the electrochemical capacity of the cathodes at 25 °C using LAND-CT2001A instrument with a charge and discharge current density of 50 mA g^{-1}, as well as with various current densities for investigating rate capability. The cut-off potentials for charge and discharge processes were set at 2.5 and 0.8 V (vs. Li/Li^+). The cyclic voltammetry (CV) measurement was conducted with a CHI 600A electrochemical workstation at a scan rate of 0.1 mV s^{-1}. Electrochemical impedance experiments were conducted using Zahner IM6ex electrochemical workstation with 5 mV amplitude of perturbation in the frequency range of 100 kHz–10 mHz. The samples were also investigated after different cycles under the current density of 50 mA g^{-1}.

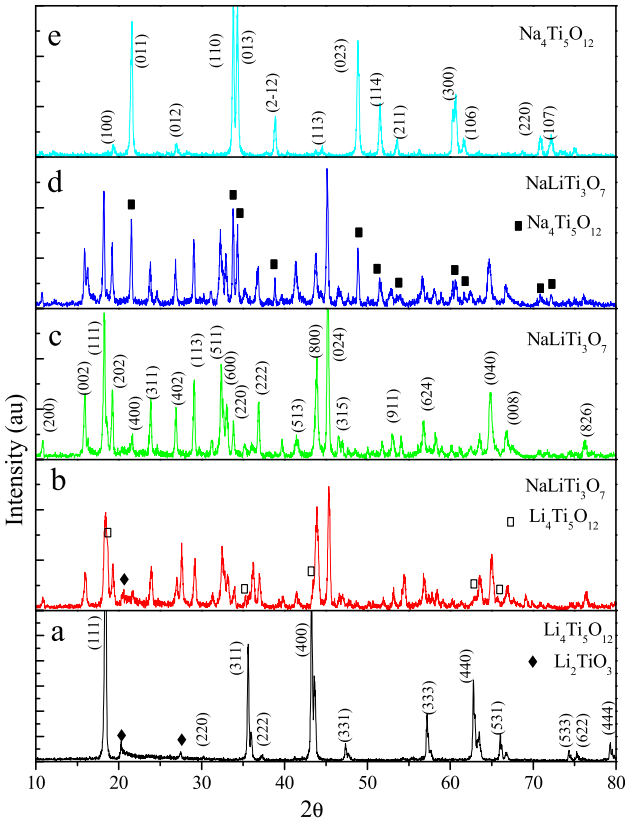

Fig. 1. XRD patterns of the as-prepared samples. (a) $Li_4Ti_5O_{12}$, (b) $Li_3NaTi_5O_{12}$, (c) $Li_2Na_2Ti_5O_{12}$, (d) $LiNa_3Ti_5O_{12}$, and (e) $Na_4Ti_5O_{12}$.

3. Results and discussion

3.1. Structure and morphology

Fig. 1 shows XRD patterns of the as-prepared samples. It is clear that the structure transformation is detected with increasing the molar ratio of sodium ions to lithium ions in the as-prepared $Li_{4-x}Na_xTi_5O_{12}$ samples. In the case of $Li_4Ti_5O_{12}$, the cubic phase of $Li_4Ti_5O_{12}$ spinel (JCPDS 49-0207) is dominant, accompanied with a trace of monoclinic Li_2TiO_3 (JCPDS 71-2348) as intermediate product, which usually coexists with $Li_4Ti_5O_{12}$ spinel in low temperature by solid state synthesis [35]. When one mole of lithium ions is substituted by sodium ions, designated as $Li_3NaTi_5O_{12}$, three crystalline phases appear in the resulting sample: dominant $NaLiTi_3O_7$ phase with an orthorhombic structure (JCPDS 52-0690), a small fraction of $Li_4Ti_5O_{12}$, and a trace of Li_2TiO_3 phase. With increasing the molar ratio of lithium ions to sodium ions (1:1), designated as $Li_2Na_2Ti_5O_{12}$, the sample is indexed to pure $NaLiTi_3O_7$ with an orthorhombic structure, highly matched in both peak position and intensity in the XRD pattern. The final composition is not identical to the elemental molar ratio used in starting materials, however, it can easily be understood in terms of volatility of the lithium carbonate. When the molar ratio of lithium ions to sodium ions is increased to 3:1, $LiNa_3Ti_5O_{12}$, the $NaLiTi_3O_7$ phase and $Na_4Ti_5O_{12}$ phase coexist. As expected, when lithium ions are completely substituted by sodium ions, pure $Na_4Ti_5O_{12}$ with a hexagonal structure (JCPDS 52-1814) can be obtained stoichiometrically. The results show that pure $NaLiTi_3O_7$ with an orthorhombic structure can be formed in the high temperature solid-phase reaction when sodium and lithium coexist in the starting materials under the used conditions. In the $NaLiTi_3O_7$ structure, the intercalated edge and corner-sharing distorted TiO_6 octahedra are

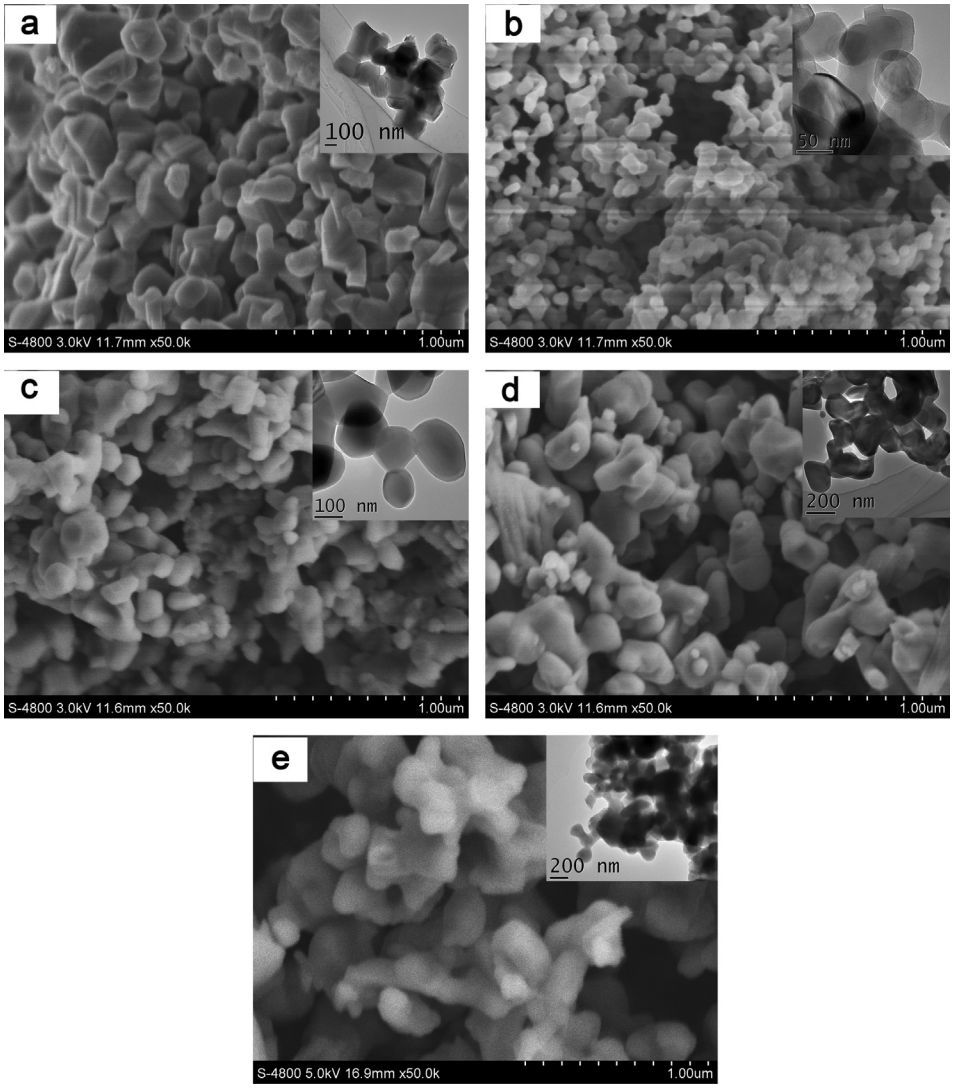

Fig. 2. SEM and TEM images of the as-prepared samples. (a) $Li_4Ti_5O_{12}$, (b) $Li_3NaTi_5O_{12}$, (c) $Li_2Na_2Ti_5O_{12}$, (d) $LiNa_3Ti_5O_{12}$, and (e) $Na_4Ti_5O_{12}$.

arranged, which provide a relatively open tunnel structure along the *b*-axis for the lithium insertion/extraction and the lithium ion diffusion [31].

SEM and TEM images of the as-prepared samples are shown in Fig. 2. The average crystallite sizes of the as-prepared $Li_4Ti_5O_{12}$ and $Na_4Ti_5O_{12}$ samples are 200–300 nm, respectively. The crystallite size of the Na/Li-coexisted samples is smaller than that of the $Li_4Ti_5O_{12}$ and $Na_4Ti_5O_{12}$ samples because the addition of heterogeneous atoms in the host lattice retards the sintering between primary grains [36]. In the as-prepared $Li_{4-x}Na_xTi_5O_{12}$ samples, it is clear that the crystallite size of all the samples is homogenously distributed and increased gradually with increasing the molar ratio of sodium ions to lithium ions in the samples. The $Li_3NaTi_5O_{12}$ sample is composed of regular nano-particles with a diameter of 70–100 nm as shown in TEM image. In the $Li_2Na_2Ti_5O_{12}$ sample, the crystallite size is increased to 100–200 nm. With further increasing the molar ratio of sodium ions to lithium ions, the crystallites are inclined to merge into big and irregular aggregates. The crystallite size is about 150–250 nm for the $LiNa_3Ti_5O_{12}$ sample. It means that the substitution of lithium ions by sodium ions has a great impact on the crystalline size of in the as-prepared $Li_{4-x}Na_xTi_5O_{12}$ samples, and sodium ions here seem to be beneficial to the growth of the crystallites.

3.2. Electrochemical performances

The initial discharge curves of the as-prepared samples at the current density of 50 mA g^{-1} are shown in Fig. 3. The initial discharge capacities of the as-prepared $Li_3NaTi_5O_{12}$ and $Li_2Na_2Ti_5O_{12}$ samples are 131.8 and 131.6 mAh g^{-1}, respectively, lower than that (157.6 mAh g^{-1}) of $Li_4Ti_5O_{12}$. The more dramatic change is shown in the discharge potential plateau when lithium ions are gradually substituted by sodium ions in $Li_4Ti_5O_{12}$. Clearly, the flat potential plateau of $Li_4Ti_5O_{12}$ is about 1.55 V (vs Li/Li^+) in the initial discharge process, corresponding to two-phase reaction between $Li_4Ti_5O_{12}$ and $Li_7Ti_5O_{12}$ [5]. When one mole of lithium ions is substituted by sodium ions ($Li_3NaTi_5O_{12}$), the midpoint potential is shown to reduce to 1.24 V (vs Li/Li^+) in the sloped discharge curve, much lower than that of $Li_4Ti_5O_{12}$. In addition, the upper and short discharge potential plateau appears in 1.54 V (vs Li/Li^+) and the short charge potential plateau can be found in 1.60 V (vs Li/Li^+), which are attributed to the presence of $Li_4Ti_5O_{12}$ in the $Li_3NaTi_5O_{12}$ sample as demonstrated in XRD patterns. In the case of the $Li_2Na_2Ti_5O_{12}$ sample, the upper and short discharge potential plateau disappears, and only sloped discharge curve with the low midpoint potential of 1.21 V (vs Li/Li^+) is presented, which is in consistent with the existence of the single phase $Li_2Na_2Ti_5O_{12}$. It

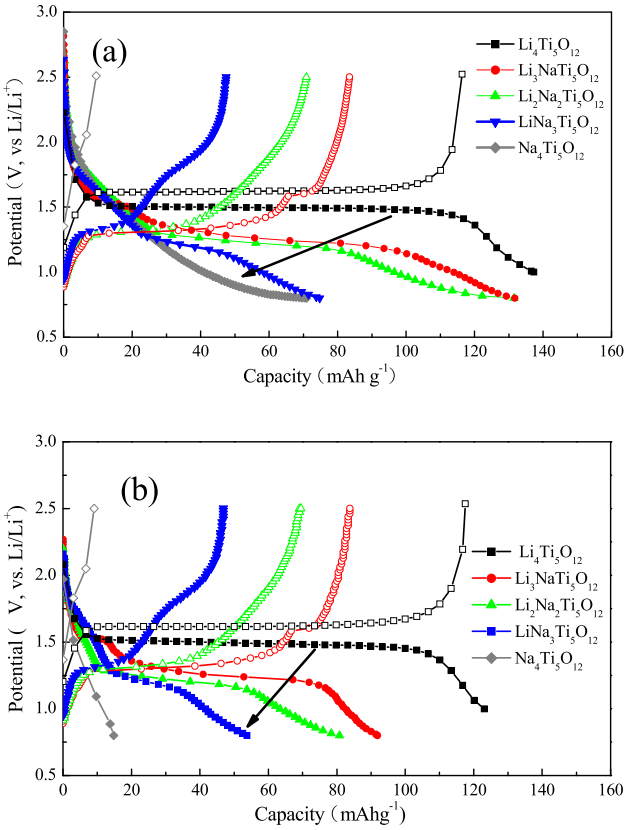

Fig. 3. The charge–discharge curves of the as-prepared samples in (a) the initial and (b) second cycle at the current density of 50 mA g^{-1}.

should be noted that the sloped discharge curve is mainly related to the solid solution lithium insertion/extraction processes in a relatively open tunnel structure. With further substitution of lithium ions by sodium ions, both the midpoint potential and discharge capacity are decreased. In the second cycle, the almost identical change of the discharge potential plateaus for all the samples is still observed, accompanied with the decrease of the discharge capacities. It implies that there is irreversible capacity loss during the formation of the solid electrolyte interface (SEI) film in the initial discharge process. The similar phenomena usually appear for Ti-based nanoparticles due to the existence of irreversible Li insertion sites and trace water adsorbed on the surface of active materials [9,36].

To illuminate the effect of the partial substitution of lithium ions by sodium ions in $Li_4Ti_5O_{12}$, the cyclic voltammograms of the as-prepared samples are measured at the scan rate of 0.1 mV s^{-1}, as presented in Fig. 4. There is only a pair of sharp redox peaks for the as-prepared $Li_4Ti_5O_{12}$ sample, consistent with the couple of the discharge/charge potential plateaus as mentioned above. For the $Li_3NaTi_5O_{12}$ sample, there are two pairs of redox peaks in the cathodic and anodic processes, located at around 1.50/1.59 V and 1.15/1.37 V (vs Li/Li^+), respectively, corresponding to the appearance of the two potential plateaus in the discharge/charge processes as shown in Fig. 3. In the second cycle, the peak intensity in the cathodic process is slightly decreased, in line with the loss in the discharge capacity. On the contrary, the peak shape in the anodic process remains unchanged almost, indicating the good reversible capability and stability. In the case of the $Li_2Na_2Ti_5O_{12}$ sample, only a pair of redox peaks at around 1.11/1.38 V (vs Li/Li^+) appears in the cathodic and anodic processes, in agreement with the presence of the one potential plateau in the discharge and charge processes, respectively. When the molar ratio of lithium ions to sodium ions is increased to 3:1 ($LiNa_3Ti_5O_{12}$), the peak intensity is obviously lower, leading to the decrease in the charge and discharge capacities. Meanwhile, two pairs of redox peaks can be observed due to the coexistence of the $NaLiTi_3O_7$ phase and $Na_4Ti_5O_{12}$ phase as shown in XRD patterns. Comparing with the cathodic peaks in CV profiles of the three materials, it is clear that there are some important features for the single phase $Li_2Na_2Ti_5O_{12}$ sample. Importantly, the cathodic and anodic peak potentials are obviously lower for anode, which are responsible for insuring the high working voltage of lithium ion batteries.

The rate discharge capability and cycle stability of the as-prepared samples are investigated at various current densities from 50 to 1500 mA g^{-1} as shown in Fig. 5. At the low current density of 150 mA g^{-1} after 10 cycles, $Li_4Ti_5O_{12}$, $Li_3NaTi_5O_{12}$, $Li_2Na_2Ti_5O_{12}$ and $LiNa_3Ti_5O_{12}$ deliver stable discharge capacities of 117.1, 65.2 and 46.1 mAh g^{-1}, respectively. With increasing the current density to 300 mA g^{-1}, the decrease of discharge capacities is not serious for all the four samples. When the current density is increased up to 1500 mA g^{-1}, the difference in the discharge capacity is obvious. In comparison of the Na/Li-coexisted samples, the

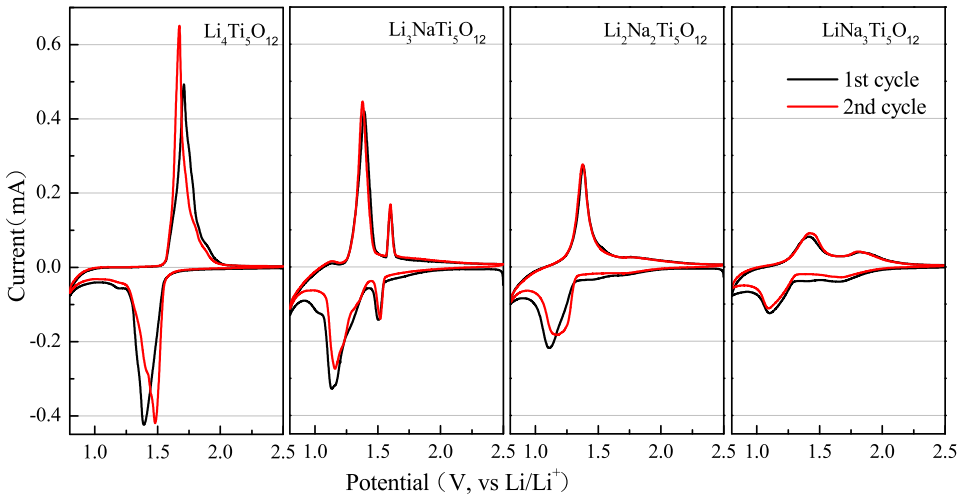

Fig. 4. Cyclic voltammograms of the as-prepared $Li_4Ti_5O_{12}$, $Li_3NaTi_5O_{12}$, $Li_2Na_2Ti_5O_{12}$ and $LiNa_3Ti_5O_{12}$ at a scan rates of 0.1 mV s^{-1}.

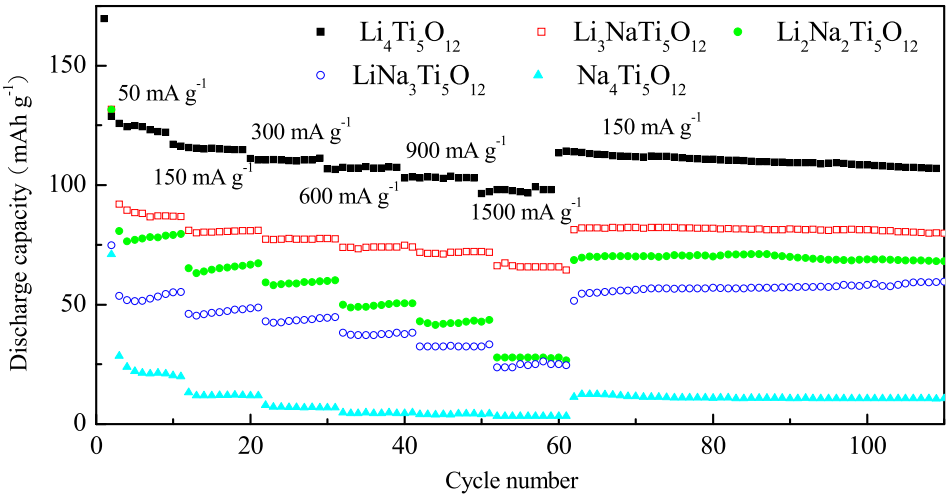

Fig. 5. Cycle performance of the as-prepared samples at various current densities.

$Li_3NaTi_5O_{12}$ presents the high discharge capacity and excellent rate capability. The abundant grain interface in the multi-phase $Li_3NaTi_5O_{12}$ sample is contributed to such excellent rate capability [37]. More importantly, after 60 cycles at varied discharge current densities, all the three samples deliver the high discharge capacity at the current density of 150 mA g^{-1}, respectively, slightly larger than the value in the 20th cycle. It is noted that all the three samples can endure great changes of various low or high discharge current densities to retain high stability upon cycling, which is beneficial for the abuse tolerance of lithium-ion batteries with the high power and long stability. On the contrary, the rate discharge capability of the $Na_4Ti_5O_{12}$ is poor, similar to the discharge performance in the low current density in Fig. 3. Therefore, the suitable substitution of lithium ions by sodium ions in $Li_4Ti_5O_{12}$ is absolutely necessary for improving the electrochemical performance, including the potential plateau, discharge capacity and high-rate capability.

Electrochemical impedance spectra (EIS) of the as-prepared materials are measured as shown in Fig. 6, before discharge, after 1st, 5th and 10th cycles. Before discharge and after 1st cycle, all the samples present the similar EIS plots, which are consisted with a semicircle in the high-frequency region and a straight line in the low-frequency region. The semicircle in the high-frequency region is mainly related to surface charge-transfer process, and straight line in the low-frequency region corresponds to a semi-infinite Warburg diffusion process. However, after 5th and 10th cycles, one small semicircle divided in the high-frequency region appears in the spectra, which is attributed to the gradual formation of the solid-electrolyte interface (SEI) film after suffering several cycles [38]. EIS spectra are simulated using the equivalent circuit inserted in Fig. 6, and the simulated values are summarized in Table 1. Here, R_s, R_f, R_{ct} and W are denoted as the solution resistance, SEI film resistance, surface charge-transfer resistance and Warburg diffusion impedance, respectively. Obviously, the surface charge-transfer resistance and Warburg diffusion impedance are dominant in the electrode reaction processes for all the samples. In addition, the surface charge-transfer resistance and Warburg diffusion impedance are steadily enhanced with increasing the molar ratio of sodium ions to lithium ions in the samples after the 1st cycle. These two dominant parameters are highly responsible for the high-rate discharge capability of the electrodes in Fig. 5. After further cycling, the surface charge-transfer resistance tends to decrease, accompanied with the formation of the SEI film. It means that more active sites are produced in the repeatedly lithium insertion/extraction processes. In the Na/Li-coexisted samples, the multi-phase $Li_3NaTi_5O_{12}$ sample presents the low surface charge-transfer resistance and Warburg diffusion impedance due to the abundant interface structure [37], which is the intrinsic reason for improving the high-rate capability. More sodium ion substitution in the samples would block the lithium ion diffusion in the bulk, leading to the increase of the Warburg diffusion impedance.

To demonstrate the formation of the SEI film, HRTEM images of the as-prepared $Li_2Na_2Ti_5O_{12}$ before and after 10 cycles are measured and indicated in Fig. 7. For the as-prepared sample, a continuous interference fringe spacing (0.48 nm) of (111) plane with a good crystallinity is found until the clear grain edge (Fig. 7a). After 10 cycles, a thin amorphous film with a thickness of 3–5 nm is clearly shown on the top surface of the grain edge based on their mass contrast, which is formed in the low potential region during the discharge process. Beneath the amorphous SEI film, the interference fringes in the bulk are still intact without any defects, such dislocations and disordered domains. Therefore, the formation of the stable thin SEI film on the grain surface is highly important for insuring the good cycle stability of the as-prepared $Li_2Na_2Ti_5O_{12}$ sample.

Actually, the substitution of lithium ions by sodium ions in $Li_4Ti_5O_{12}$ has the great impact on the structure, crystalline size and electrochemical performance. When lithium ions are partially substituted by sodium ions, the relatively open tunnel structure supported by the larger sodium ions in the host material can be formed, which is beneficial for decreasing the operation potential in the lithium insertion/extraction processes. Of course, the decrease of the operation potential is obtained at the expense of the discharge capacity due to the substitution by heavy sodium ions. From the results as mentioned above, the half substitution of lithium ions by sodium ions is available based on the evaluation of the potential plateau, discharge capacity and high-rate capability.

4. Conclusion

In conclusion, lithium ions are substituted gradually by sodium ions in the as-prepared $Li_{4-x}Na_xTi_5O_{12}$ samples, prepared by the high temperature calcination of titania and anhydrous lithium carbonate and anhydrous sodium carbonate. With gradually increasing the molar ratio of sodium ions to lithium ions in the as-prepared $Li_{4-x}Na_xTi_5O_{12}$ samples, the phase structure is obviously converted to an orthorhombic structure ($NaLiTi_3O_7$) from a cubic

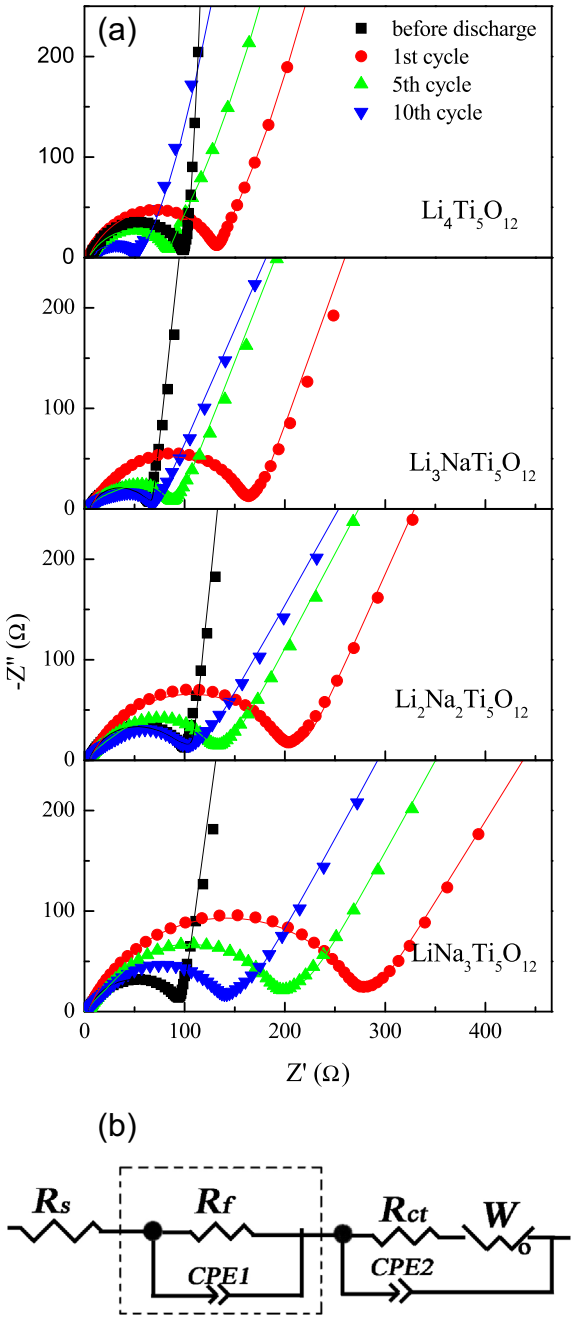

Fig. 6. (a) Nyquist plots of the as-prepared $Li_4Ti_5O_{12}$, $Li_3NaTi_5O_{12}$, $Li_2Na_2Ti_5O_{12}$ and $LiNa_3Ti_5O_{12}$ under open circuit condition at the charged state after various cycles (50 mA g^{-1}). The symbols and lines correspond to the experimental and simulated data, respectively. (b) The used equivalent circuit, in which the elements in the dashed frame are only involved for fitting the 5th and 10th cycle spectra.

structure, and finally to a hexagonal structure ($Na_4Ti_5O_{12}$). Meanwhile, the crystalline size of the samples is increased with more sodium ion substitution. Although the discharge capacity is slightly decreased with sodium ion substitution in the samples, as expected, the lower potential plateau is indeed obtained in the Na-ion substituted samples. In particular, the single phase $Li_2Na_2Ti_5O_{12}$ sample presents one low and sloped potential plateau, which is responsible for insuring the high working voltage of lithium ion batteries. Therefore, the suitable substitution of lithium ions by sodium ions in $Li_4Ti_5O_{12}$ is absolutely necessary for improving the

Table 1
The simulated data from EIS spectra using the equivalent circuit shown in Fig. 6.[a]

Sample	Cycle	R_s (Ω)	R_f (Ω)	R_{ct} (Ω)	W (Ω)
$Li_4Ti_5O_{12}$	0	6.8	–	88.3	30.0
	1st	4.6	–	121.5	50.4
	5th	4.5	85.1	94.4	54.0
	10th	8.0	46.6	48.1	52.0
$Li_3NaTi_5O_{12}$	0	5.2	–	58.0	15.0
	1st	6.1	–	150.2	44.8
	5th	4.7	45.8	30.0	36.5
	10th	4.9	33.8	22.7	31.4
$Li_2Na_2Ti_5O_{12}$	0	4.7	–	91.09	39.7
	1st	5.2	–	194.7	56.3
	5th	4.7	35.7	77.6	78.2
	10th	4.4	33.7	48.5	88.3
$LiNa_3Ti_5O_{12}$	0	3.5	–	87.8	22.5
	1st	3.7	–	258.0	84.6
	5th	3.9	19.8	150.3	120.0
	10th	4.0	16.0	103.5	104.3

[a] R_s: solution resistance; R_{ct}: charge transfer resistance; R_f: SEI film resistance; W: Warburg diffusion impedance.

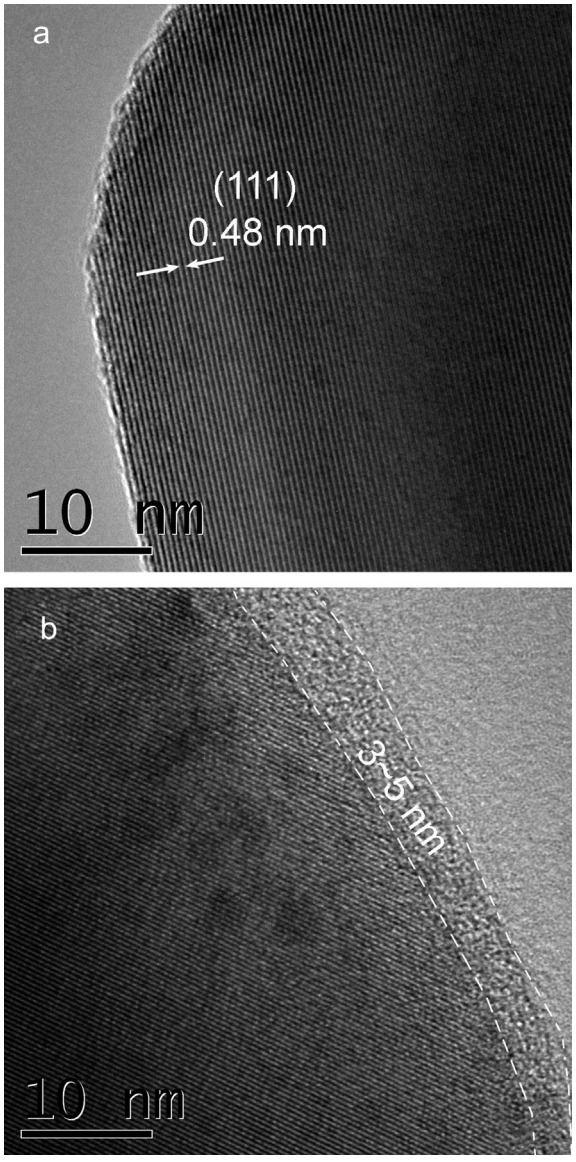

Fig. 7. TEM images of the as-prepared $Li_2Na_2Ti_5O_{12}$ before and after 10 cycles at the current density of 50 mA g^{-1}.

electrochemical performance, including the potential plateau, discharge capacity and high-rate capability.

Acknowledgments

Financial support from the 973 Program (2009CB220100) is greatly appreciated.

References

[1] T.H. Kim, J.S. Park, S.K. Chang, S. Choi, J.H. Ryu, H.K. Song, Adv. Energy Mater. 2 (2012) 860.
[2] L. Xia, S.L. Li, X.P. Ai, H.X. Yang, Y.L. Cao, Energy Environ. Sci. 4 (2011) 2845.
[3] L. Zhang, Z.C. Zhang, P.C. Redfern, L.A. Curtiss, K. Amine, Energy Environ. Sci. 5 (2012) 8204.
[4] T. Ohzuku, A. Ueda, N. Yamamoto, J. Electrochem. Soc. 142 (1995) 1431.
[5] S. Scharner, W. Weppner, P. Schmid-Beurmann, J. Electrochem. Soc. 146 (1999) 857.
[6] G.N. Zhu, Y.G. Wang, Y.Y. Xia, Energy Environ. Sci. 5 (2012) 6652.
[7] Y.F. Tang, L. Yang, Z. Qiu, J.S. Huang, J. Mater. Chem. 19 (2009) 5980.
[8] Y. Li, G.L. Pan, J.W. Liu, X.P. Gao, J. Electrochem. Soc. 156 (2009) A495.
[9] C. Lai, Y.Y. Dou, X. Li, X.P. Gao, J. Power Sources 195 (2010) 3676.
[10] G.J. Wang, J. Gao, L.J. Fu, N.H. Zhao, Y.P. Wu, T. Takamura, J. Power Sources 174 (2007) 1109.
[11] G.N. Zhu, C.X. Wang, Y.Y. Xia, J. Electrochem. Soc. 158 (2011) A102.
[12] D.W. Liu, G.Z. Cao, Energy Environ. Sci. 3 (2010) 1218.
[13] H.G. Jung, S.T. Myung, C.S. Yoon, S.B. Son, K.H. Oh, K. Amine, B. Scrosati, Y.K. Sun, Energy Environ. Sci. 4 (2011) 1345.
[14] X.B. Hu, Z.J. Lin, K.R. Yang, Y.J. Huai, Z.H. Deng, Electrochim. Acta 56 (2011) 5046.
[15] H.G. Jung, J. Kim, B. Scrosati, Y.K. Sun, J. Power Sources 196 (2011) 7763.
[16] B. Zhang, Y.S. Liu, Z.D. Huang, S. Oh, Y. Yu, Y.W. Mai, J.K. Kim, J. Mater. Chem. 22 (2012) 12133.
[17] Y.R. Jhan, J.G. Duh, J. Power Sources 198 (2012) 294.
[18] L.F. Shen, X.G. Zhang, E. Uchaker, C.Z. Yuan, G.Z. Cao, Adv. Energy Mater. 2 (2012) 691.
[19] B.H. Li, C.P. Han, Y.B. He, C. Yang, H.D. Du, Q.H. Yang, F.Y. Kang, Energy Environ. Sci. 5 (2012) 9595.
[20] R.Y. Wang, J. Wang, T. Qiu, L.P. Chen, H.M. Liu, W.S. Yang, Electrochim. Acta 70 (2012) 84.
[21] I. Belharouak, Y.K. Sun, W. Lu, K. Amine, J. Electrochem. Soc. 154 (2007) A1083.
[22] A. Jaiswal, C.R. Horne, O. Chang, W. Zhang, W. Kong, E. Wang, T. Chern, M.M. Doeff, J. Electrochem. Soc. 156 (2009) A1041.
[23] J.H. Kim, S.Y. Bae, J.H. Min, S.W. Song, D.W. Kim, Electrochim. Acta 78 (2012) 11.
[24] H.M. Wu, I. Belharouak, H. Deng, A. Abouimrane, Y.K. Sun, K. Aminea, J. Electrochem. Soc. 156 (2009) A1047.
[25] S.K. Martha, O. Haik, V. Borgel, E. Zinigrad, I. Exnar, T. Drezen, J.H. Miners, D. Aurbach, J. Electrochem. Soc. 158 (2011) A790.
[26] X.K. Huang, M. Lin, Q.S. Tong, X.H. Li, Y. Ruan, Y. Yang, J. Power Sources 202 (2012) 352.
[27] S.W. Kim, D.H. Seo, X.H. Ma, G. Ceder, K. Kang, Adv. Energy Mater. 2 (2012) 710.
[28] S.H. Huang, Z.Y. Wen, X.J. Zhu, Z.X. Lin, J. Power Sources 165 (2007) 408.
[29] L.M. Torres-Martinez, J. Ibarra, J.R. Loredo, L.L. Garza-Tovar, O. Martinez-Bruno, Solid State Sci. 8 (2006) 1281.
[30] R. Dominko, E. Baudrin, P. Umek, D. Arcon, M. Gaberscek, J. Jamnik, Electrochem. Commun. 8 (2006) 673.
[31] S.Y. Yin, L. Song, X.Y. Wang, Y.H. Huang, K.L. Zhang, Y.X. Zhang, Electrochem. Commun. 11 (2009) 1251.
[32] S.H. Woo, Y. Park, W.Y. Choi, N.S. Choi, S. Nam, B. Park, K.T. Lee, J. Electrochem. Soc. 159 (2012) A2016.
[33] C.H. Chen, J.T. Vaughey, A.N. Jansen, D.W. Dees, A.J. Kahaian, T. Goacher, M.M. Thackeray, J. Electrochem. Soc. 148 (2001) A102.
[34] S.Z. Ji, J.Y. Zhang, W.W. Wang, Y. Huang, Z.R. Feng, Z.T. Zhang, Z.L. Tang, Mater. Chem. Phys. 123 (2010) 510.
[35] I. Veljkovic, D. Poleti, Sci. Sintering 43 (2011) 343.
[36] H. Song, S.W. Yun, H.H. Chun, M.G. Kim, K.Y. Chung, H.S. Kim, B.W. Cho, Y.T. Kim, Energy Environ. Sci. 5 (2012) 9903.
[37] X. Li, C. Lai, C.W. Xiao, X.P. Gao, Electrochem. Acta 56 (2011) 9152.
[38] Y. Ding, G.R. Li, C.W. Xiao, X.P. Gao, Electrochem. Acta 102 (2013) 282.